

Probability density function of in-plane permeability of fibrous media: Constant Kozeny coefficient

M. Bodaghi^a, S. Yasaei Sekeh^b, N. Correia^{c,*}

^a Engineering Design and Advanced Manufacturing, MIT Portugal Program,
Faculty of Engineering, University of Porto, Porto, Portugal

^b Department of Statistics, Federal University of São Carlos, SP, Brazil

^c Institute of Mechanical Engineering and Industrial Management,
Faculty of Engineering, University of Porto, Porto, Portugal

Abstract

Permeability of fibrous porous media at the micro/meso scale-level is subject to significant uncertainty due to the heterogeneity of the fibrous media. The local microscopic heterogeneity and spatial variability porosity, tortuosity and fibre diameter affect the experimental measurements of permeability at macroscopic level. This means that the selection of an appropriate probability density function (PDF) is of crucial importance, in the characterization of both local variations at the microscale and the equivalent permeability at the experimental level (macroscale). This study addresses the issue of whether or not a normal distribution appropriately represents permeability variations. To do so, (i) the distribution of local fibre volume fraction for each tow is experimentally determined by estimation of each pair of local areal density and thickness, (ii) the Kozeny-Carmen equation together with the change of variable technique are used to compute the PDF of permeability, (iii) using the local values of fibre volume fraction, the distribution of local average permeability is computed and subsequently the goodness of fit of the computed PDF is compared with the distribution of the permeability at microscale level. Finally variability of local permeability at the microscale level is determined.

The first set of results reveals that (1) the relationship between the local areal density and local thickness in a woven carbon-epoxy composite is modelled by a bivariate normal distribution, (2) while fibre volume fraction follows a normal distribution, permeability follows a gamma distribution, (3) this work also shows that there is significant agreement between the analytical approach and the simulation results. The second set of results shows that the coefficient of variation of permeability

* Corresponding author: E-mail: nuno.correia@inegi.up.pt, Tel: (+351-229578710)

is one order of magnitude larger than that of fibre volume fraction. Future work will consider other variables, such as type of fabrics, the degree of fibre preform compaction to determine whether or not the bivariate normal model is applicable for a broad range of fabrics.

1 Introduction

Fibrous media display different degrees of meso-scale variability from ideal fibre paths. This can be due to the manufacturing of the reinforcement, handling and preparing the moulding step. Resin flow inside porous media is influenced by fibres spatial variability and heterogeneity, and neglecting this causes errors in process analysis and uncertainty in measurement. Thus a reliable model of fluid flow in heterogeneous media must include multiscale phenomena and capture the multiscale nature of fluid transport behaviour, at microscale, mesoscale and macroscale. In the sense the dominant processes and governing equations may vary with scales. Therefore, extending from microscale level to a mesoscale one needs upscaling that allows the essence of physical processes at one level to be summarized at the larger level. However, a detailed understanding of upscaling process from microscale to mesoscale has not been completed. Mesoscopic and macroscopic properties of fibrous media such as porosity, fibre size distribution and permeability can be characterized through lab-scale methods while the microscale properties are uncaptured. The lack of ability for measurements on the microscale can lead to uncertainty in interpretations of the data captured at macroscale. A major challenge arising from this non homogeneity is how macroscale flow is influenced by the microscale structure (pore spaces), as well as by the physical properties of the resin. Permeability is an important macroscale variable representing average of microscale properties of porous media. This average permeability is the fundamental property arising from Darcy's law (1):

$$\bar{u} = \frac{K}{\mu} \cdot \Delta p, \quad (1\text{D version of the equation}) \quad (1)$$

which describes the relation between the volume averaged fluid velocity, \bar{u} , the pressure gradient, Δp , the fluid's viscosity, μ , and the equivalent permeability tensor K . Empirical equations, such as Kozeny–Carmen (2), have been developed to relate the meso-scale permeability with the microscale properties, including porosity:

$$K = \frac{r_f^2}{k_c} \frac{(1 - V_f)^3}{(V_f)^2}. \quad (2)$$

Here $k_c = C\tau^2$ and $\tau^2 = \frac{L_e}{L}$, where V_f is porosity, r_f is fibre radius, k_c is Kozeny constant, τ is tortuosity, L_e is the length of streamlines, L is the length of sample and C is a proportionality constant [1].

Because the nonhomogeneous nature of porous media originates in the randomness of fibre diameter distributions, porosities and pore structure, permeability is subjected to uncertainty [2]. Causes and

effects of this uncertainty have been reviewed [3, 4], assuming a normal [4, 5, 6, 7, 8, 9, 10, 11] and a lognormal permeability probability density function [12], previous studies have modeled the effect of this uncertainty on fluid flow in porous media by employing stochastic analysis. Considered as a vast area in stochastic processes, such analyzes require to identify the sources of uncertainties and to select probabilistic methods for uncertainty propagation up to different modeling levels.

In simulation of mould filling process, such as Resin Transfer Moulding, which are described by Darcy's law (1), permeability directly affects filling time and flow pattern. An accurate probability density function for permeability is therefore vital for reliable simulations. A number of studies [7, 8, 9, 10, 11, 13, 14] have used a normal probability density functions for experimentally determined permeability at macroscale. But their measurements have been mostly for small sample sizes and hence may still be the subject to experimental and statistical inaccuracy. In other words, data obtained from the experiments may not be enough to choose between two (normal or lognormal distribution) or more competing distribution functions. Furthermore, these studies ignore the effect of microscale uncertainties on macroscale permeability uncertainties.

Different approximation methods have been used to determine the impact of microscale uncertainties on macroscale permeability uncertainties, e.g, finite element based Monte Carlo and Lattice-Boltzmann methods have been used to estimate permeability and superficial velocity of representative volume elements of porous media [16, 17, 18, 4, 20]. The accuracy of the analytical methods has been debated because they have considered homogeneous periodic arrays of parallel fibres instead of random distributions. In addition, all of the modeling approaches require that either the distribution of at least one property of fibrous media or the distribution of macropores of fibrous media be known. Another criticism is that estimating permeability by curve fitting with empirical constants is known to generate significant systematic errors.

In view of the fact that finding an appropriate distribution function describing the spatial variation of permeability in fibrous media is a challenging problem. Therefore, a method that measures the microstructural variability as input for stochastic simulations is required. In the [21], we analyzed the effect of tortuosity on the variability of permeability at the average local fibre volume fraction (microscale level). We showed that the Gaussian distribution is not necessarily the most appropriate distribution for representing permeability [21]. In this study, we capture the influence of a distribution of local fibre volume fraction (V_f) on the variability of permeability. The uncertainty in this variable (e.g, V_f) propagates to a larger level and is reflected in the variability of the geometry of flow affecting the final quality of composites. In order to establish a probability density function for permeability, in this study we propose that (i) the best probability density function may be approximated for distribution of fibre volume fraction by a normal model, (ii) the values of fibre volume fraction were used to compute the

distribution of permeability applying the Kozeny-Carmen equation, (iii) we used the Kozeny-Carmen equation together with change of variable technique to determine the probability density function of permeability and subsequently the analytical approach is compared with the distribution of permeability [23] (Figure 1).

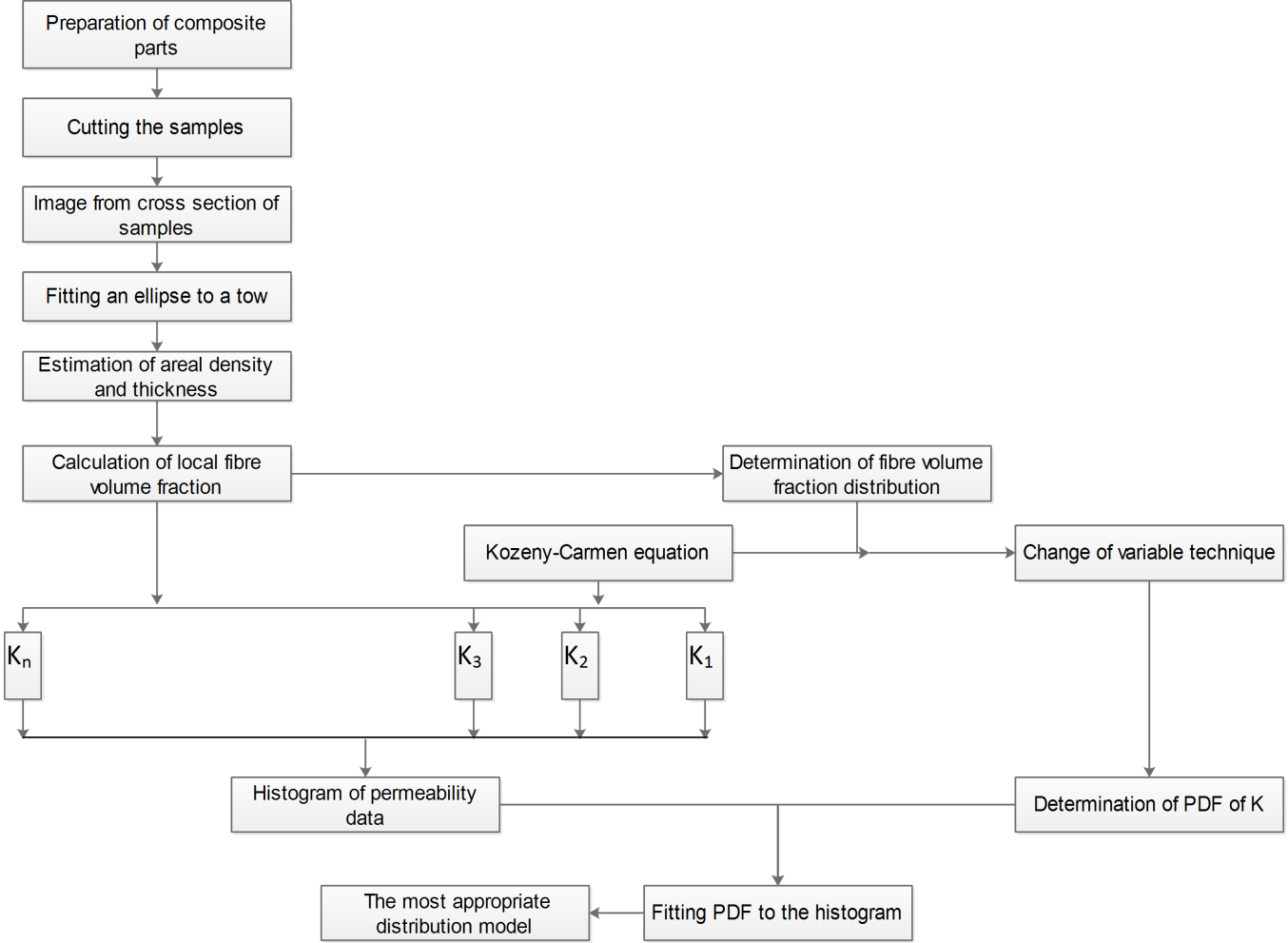


Figure 1: Flowchart for probability density function of permeability

2 The probability density function (PDF) of K

There is no universal established relationship between fibre volume fraction and permeability. In this paper we recall the Carmen Kozeny equation in order to find the PDF of permeability (2). Observe that in (2) the random variable (RV) K is an increasing function of porosity V_f (assuming r_f^2 , k_c are constant), see Figure 2. Note also that K is significantly affected by r_f^2 . However this will not be addressed in this

paper. Here we use change-of-variables technique, in this study called "the change of V_f ", to investigate PDFs of permeability. This technique is a common and well-known way of finding the PDF of $y = y(x)$ if x be a continuous random variable with a probability density function $f(x)$. Therefore to establish the PDF of random variable K , it is required to have the PDF of V_f . Thus subsequently in the next section, we determine numerically the PDF of V_f .

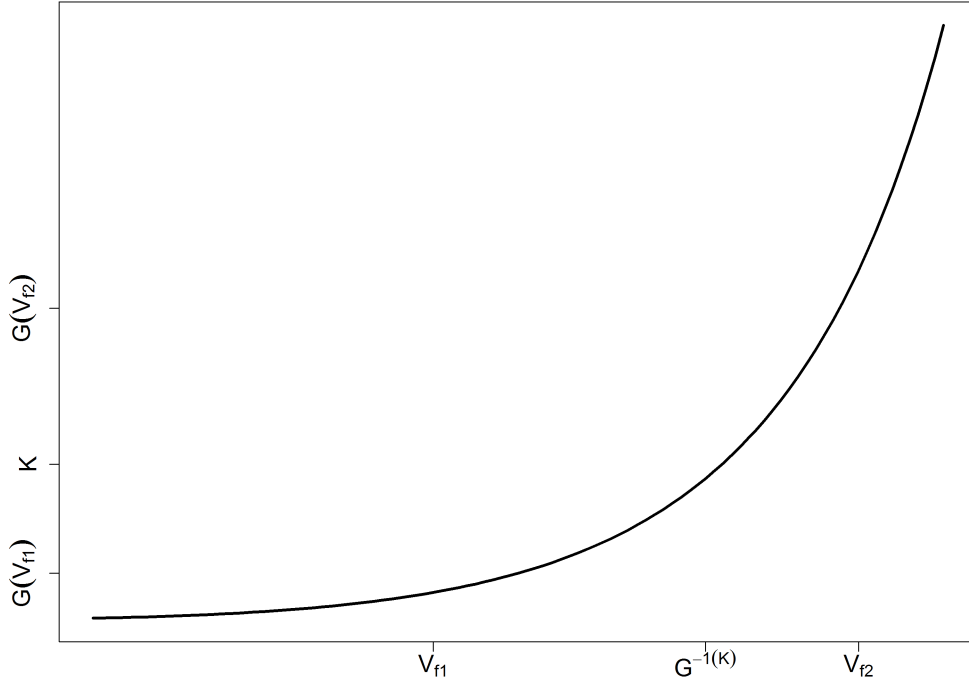


Figure 2: Continuous variation of K values as function of V_f

2.1 Fibre volume fraction (V_f)

Variable fibre volume fraction for a fibrous media depends on areal weight density (A_w) and thickness(t) and can be expressed as equation (3) :

$$V_f = \frac{A_w n}{\rho_f t} \quad (3)$$

where ρ_f stands the fibre density, n is number of layers. To attain a closed form expression of the density of V_f , both A_w and t are considered normal random variables with correlation coefficient, $-1 < \rho_{corr} < 1$. When $\rho_{corr}=0$, the two variables A_w and t are independent, the distribution of V_f would have a Cauchy

distribution. Note that the the Cauchy distribution does not have finite moments of any order hence the mean and variance of V_f are undefined. Therefore, assuming a Cauchy distribution would not be an appropriate model for fibre volume fraction. Now set $\mu_{A_w} := \mathbb{E}(A_w)$ and $\mu_t := \mathbb{E}(t)$. In this stage of work we consider the first order Taylor expansion about (μ_{A_w}, μ_t) for $V_f(A_w, t)$:

$$V_f := V_f(A_w, t) = V_f(\mu_{A_w}, \mu_t) + V'_{f_{A_w}}(\mu_{A_w}, \mu_t)(A_w - \mu_{A_w}) + V'_{f_t}(\mu_{A_w}, \mu_t)(t - \mu_t) + O(n^{-1}), \quad (4)$$

where $V'_{f_{A_w}}$ and V'_{f_t} are the derivatives of V_f with respect to A_w and t respectively. In agreement with [24, 25], the approximation for $\mu_{V_f} := \mathbb{E}(V_f)$ is given by

$$\begin{aligned} \mu_{V_f} &= \mathbb{E}\left(V_f(\mu_{A_w}, \mu_t) + V'_{f_{A_w}}(\mu_{A_w}, \mu_t)(A_w - \mu_{A_w}) + V'_{f_t}(\mu_{A_w}, \mu_t)(t - \mu_t) + O(n^{-1})\right) \\ &\approx \mathbb{E}(V_f(\mu_{A_w}, \mu_t)) + V'_{f_{A_w}}(\mu_{A_w}, \mu_t)\mathbb{E}(A_w - \mu_{A_w}) + V'_{f_t}(\mu_{A_w}, \mu_t)\mathbb{E}(t - \mu_t) \\ &= \mathbb{E}(V_f(\mu_{A_w}, \mu_t)) = n \mu_{A_w} / A_{wf} \mu_t. \end{aligned} \quad (5)$$

By virtue of the definition of variance we can write

$$\sigma^2(V_f) = \sigma^2\left(\frac{A_w}{t}\right) \left(\frac{n}{A_{wf}}\right)^2. \quad (6)$$

Next, use the first order Taylor expansion once again around (μ_{A_w}, μ_t) . Then owing to (5) we approximate

$$\sigma^2(V_f) \approx \mathbb{E}\left\{(V_f(A_w, t) - V_f(\mu_{A_w}, \mu_t))^2\right\}. \quad (7)$$

Substitute (4) in (7), then (6) becomes the following:

$$\begin{aligned} \sigma^2(V_f) &\approx \left(\frac{n}{A_{wf}}\right)^2 \sigma^2\left(\frac{\mu_{A_w}}{\mu_h} + \frac{1}{\mu_h}(\rho - \mu_\rho) - \frac{\mu_\rho}{\mu_h^2}(h - \mu_h)\right) \\ &= \left(\frac{n}{\rho_f}\right)^2 \sigma^2\left(\frac{1}{\mu_h}\rho - \frac{\mu_{A_w}t}{\mu_t^2}\right) \\ &= \left(\frac{n}{A_{wf}}\right)^2 \frac{1}{\mu_t^2} \sigma^2(A_w) + \frac{\mu_{A_w}^2}{\mu_t^4} \sigma^2(t) - 2\frac{\mu_{A_w}}{\mu_h^3} Cov(A_w, t) \\ &= \left(\frac{n}{A_{wf}}\right)^2 \frac{\mu_{A_w}^2}{\mu_t^2} \left(\frac{1}{\mu_{A_w}^2} \sigma^2(A_w) + \frac{1}{\mu_t^2} \sigma^2(t) - 2\frac{1}{\mu_{A_w}\mu_t} Cov(A_w, t)\right) \end{aligned} \quad (8)$$

In (8), $Cov(A_w, t)$ expresses the covariance of A_w , t while as we said μ_{A_w} and μ_t are average of local areal density and thickness, respectively.

Now denote $\sigma(A_w)$, $\sigma(t)$ as the standard deviation of RVs A_w , t and moreover ρ_{corr} as their correlation coefficient and their relationship can be expressed as:

$$Cov(A_w, t) = \sigma(A_w)\sigma(t)\rho_{corr}. \quad (9)$$

In addition we define the coefficient of variation (cv) of a RV, such as $cv(V_f)$:

$$cv(V_f) = \frac{\sigma(V_f)}{\mu_{V_f}} \quad (10)$$

Consequently Eqn. (8) can be recast as:

$$\sigma^2(V_f) \approx (\mu_{V_f})^2(cv^2(A_w) - 2cv(A_w)cv(t)A_{wcorr} + cv^2(t)) \quad (11)$$

Consider (11) and replace it in (10), then the cv of fibre volume fraction yields:

$$cv(V_f) \approx \sqrt{cv^2(A_w) - 2cv(A_w)cv(t)\rho_{corr} + cv^2(t)} \quad (12)$$

Equation (12) shows that the cv of RV fibre volume fraction V_f is approximately independent from μ_{V_f} . Owing to (12) at point $\mu_{V_f} = 0.5$, evidently 3D Scatter plots (3) exhibits variation of the cv of the RV fibre volume fraction V_f as a function of the coefficient of variations thickness $cv(t)$ and local areal density $cv(A_w)$.

In Figure 3, it is possible to observe that when ρ_{corr} increases from zero to one, a saddle is formed with $\rho_{corr} = 1$, $cv(A_w) = cv(t)$ and then $cv(V_f) = 0$. Furthermore, Figure 3 shows that as $cv(A_w)$ and $cv(t)$ approach each other too closely, $cv(V_f)$ moves from the top to the lowest level.

As to the PDF of V_f , section 2.1.1 establishes experimentally that the random variable V_f has normal distribution. Although by calling the following cases we claim that this assertion in independent case is not theoretically artificial:

1. A_w and t are **independent**. It is straightforward that when a random variable t follows Cauchy distribution with parameter γ then $1/t$ has also Cauchy distribution with parameter $1/\gamma$. Further, according to our explanation above, we can easily check that the ratio of two independent normal random variables determines the Cauchy PDF. Hence as result if we consider random variables A_w and t takes normal and Cauchy distributions respectively then V_f has normal PDF.
2. A_w and t are **dependent**. This case is more complicated but practical. First note that if one is interested in bivariate normal distribution for pair (A_w, t) . We address to [26] which study the ratio of two correlated normal random variables. The author indeed has established that if A_w and t be normally distributed random variables with means μ_i , variances σ_i^2 , ($i = 1, 2$) and correlated coefficient ρ_{corr} , then the exact PDF of V_f takes the form (1) in page 636 in [26]. For simplicity we omit the form (1) here. However, in [27] we could observe that in this special case, i.e. normally distributed (A_w, t) the PDF of V_f is not necessarily symmetric and normal. Therefore by virtue of author's investigations, it is not clear yet that what kind of distributions should be considered for (A_w, t) to prove analytically a normal PDF for V_f . Consequently, the solution which may come cross the mind is experimental results represented in next subsection.

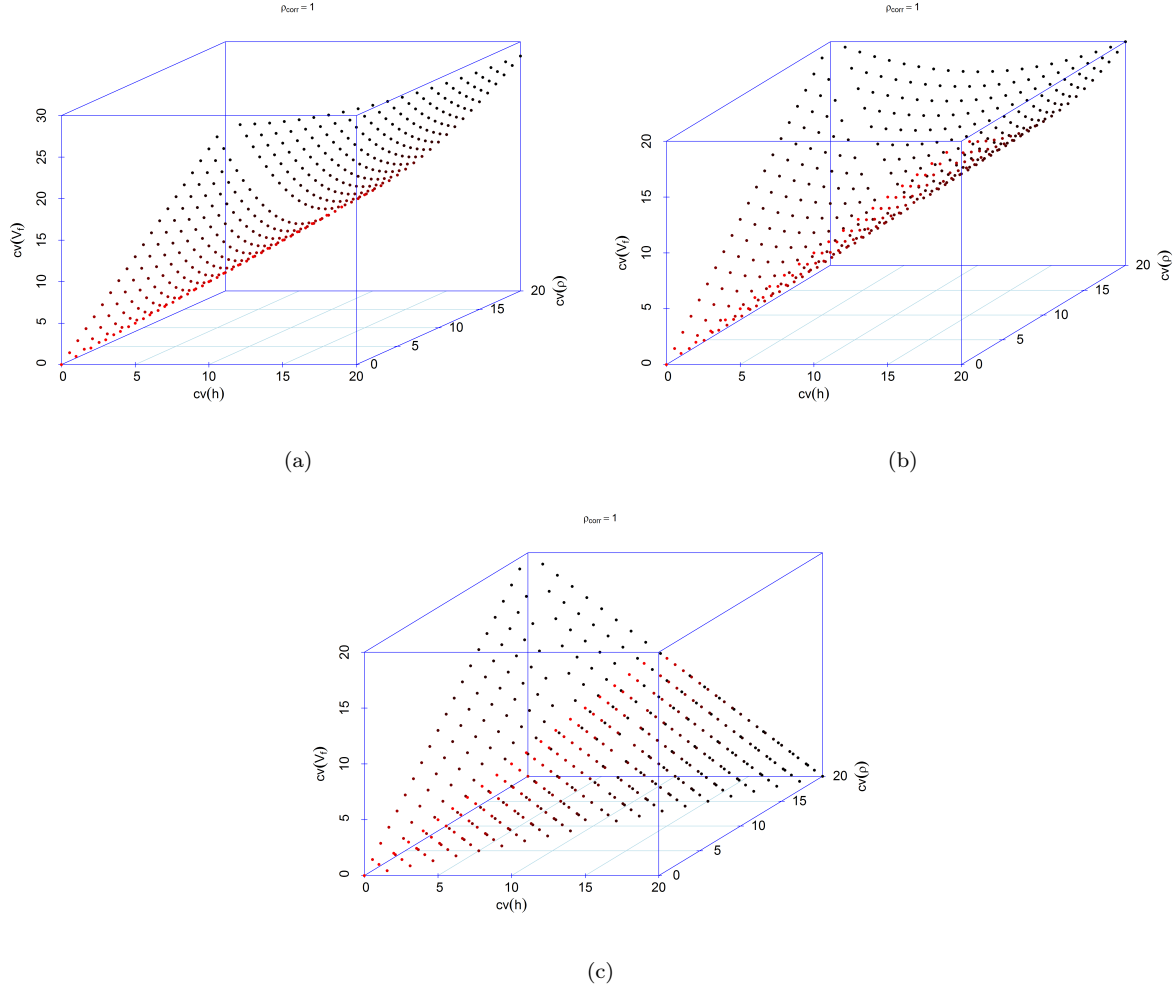


Figure 3: Coefficient of variation of fibre volume fraction $cv(V_f)$ as a function of coefficient of variation of areal density, $cv(A_w)$, and thickness, $cv(t)$, at $\mu_{V_f} = 0.5$. (a) $\rho_{corr} = 0$, (b) $\rho_{corr} = 0.5$, (c) $\rho_{corr} = 1$

2.1.1 Experimental

Table 1 shows the specifications of a 2×2 twill carbon woven fabric used for production of composite parts in this study. The Fabric was cut in the warp direction. Composite parts were produced with same V_f using High Injection Pressure Resin Transfer Moulding (HIPRTM). Full production details have been presented in [27].

In order to measure the h of each tow, series of samples were cut perpendicular to the fibre direction, the samples were polished manually in four steps (sandpaper grits 320, 400, 800, and 1000), and subsequently photographed using an Olympus PNG3 optical microscope equipped with a CCD camera. The analysis of each tow is carried out by image processing Matlab TM2015. Before importing the images into

Table 1: Material properties of fabrics used to prepare composite samples

Style	Weave pattern	Areal weight(gm^{-2})	Maximum width(cm)	Fiber diameter(μm)	Number of filaments
280T	2×2 twill	280	100	7	3000

the Matlab TM workspace, areas such as edges or borders which are not in the interest of tow geometry characterizations were cropped. In projective geometry every tow section is equivalent to an ellipse. Figure 4a illustrates how an ellipse is fitted to a tow to locate the center point based on [28] and [29]. Then the tow thickness (t) is equivalent to twice the length of the minor radius (b) (Figure 4b). A total of 200 optical images were collected and an ellipse is fitted to each tow.

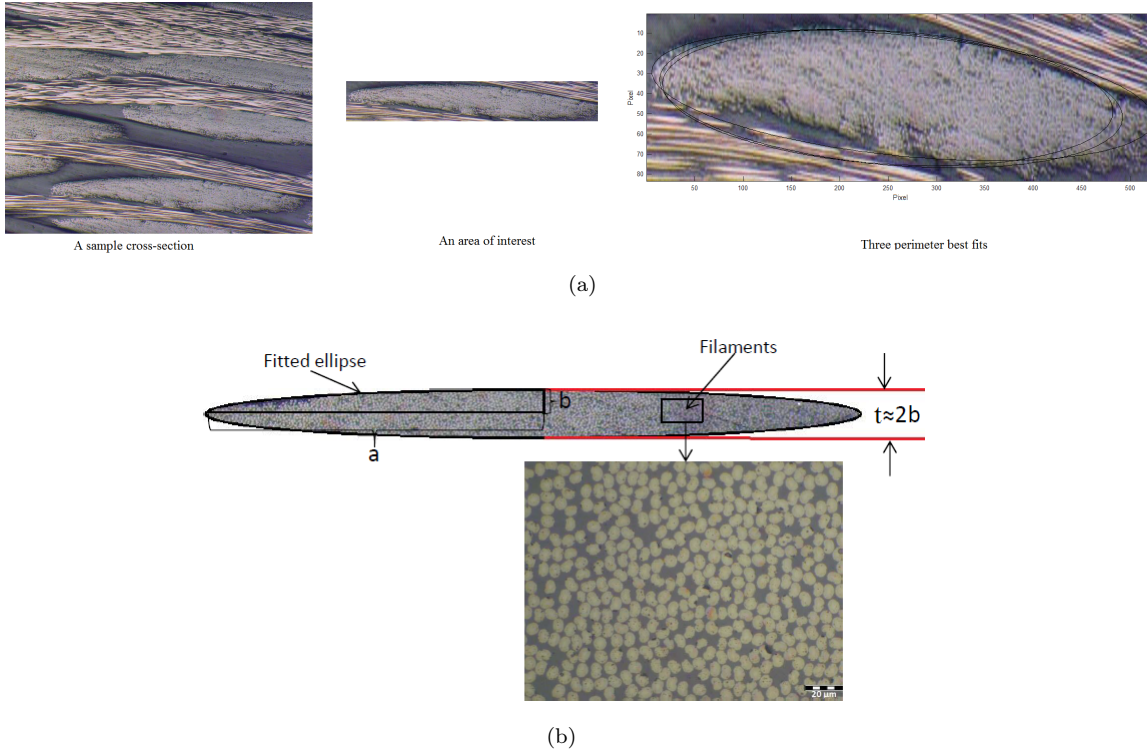


Figure 4: (a) Ellipse detection, (b) Tow geometry parameters

To determine the A_w of each tow, the area of each tow (A_t) in warp direction was approximated by the equivalent ellipse. Then, the number of filaments per tow (n_t) were counted. Knowing the radius of the fibre cross section(r), length of warp tow (l), and ρ_f , the A_w of each tow(w_t) was computed from the following equation (13):

$$A_w = \frac{n_t \pi r^2 \rho_f}{2a} \quad (13)$$

To determine distribution of V_f , the "R" statistical software [31] was employed. For each pair (t, A_w) , V_f was computed, afterward a histogram was generated .

2.1.2 Results

A scatter plot of A_w and t for each tow is shown in Figure 5. The coefficient of variation for the data was 0.72. An ellipse is fitted to the data. We can see that the ellipse extends between 100 and 200 (g/m^2) on the 45 degree line. Hence A_w and t follow a bivariate normal distribution with mean components 168.5 g/m^2 and 102.3 μm , respectively. Therefore, our results suggest that A_w and t are dependent and can be well approximated by the bivariate normal distribution.

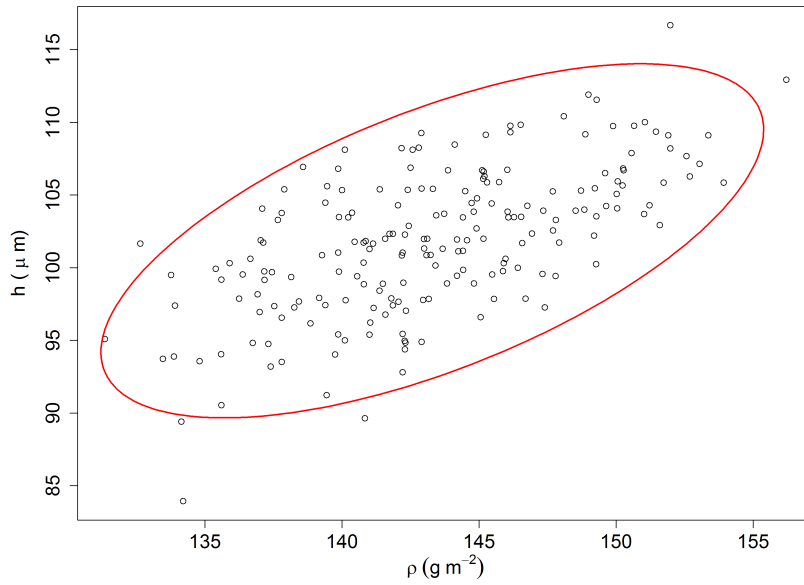


Figure 5: The relation of local average areal density with local average thickness. The bivariate normal ellipse (P=0.95) shows the data fit.

For each pair of A_w and t , V_f was computed. Figure 6 shows that the distribution of the local average fibre volume fraction follows a bell-curve distributions: the distribution of fibre volume fraction values are well approximated with a normal distribution model. A large distribution of V_f was observed, ranging from 60% to 95%. The graphical analysis indicates the closeness of the local average fibre volume fraction

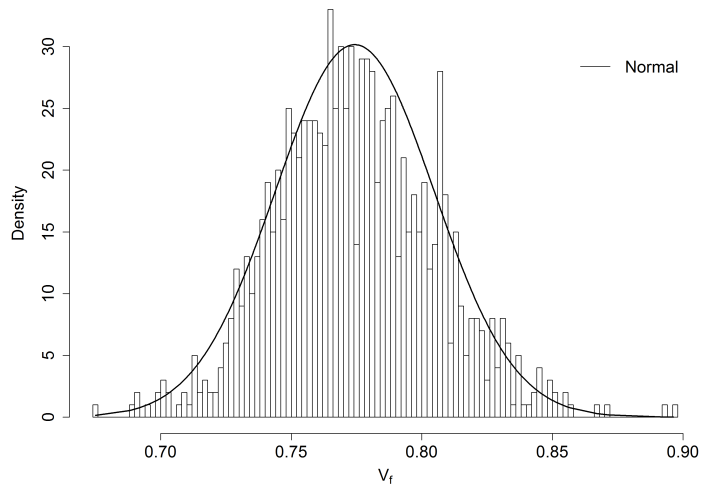


Figure 6: Distribution of the local average fibre volume fraction.

data to the normal distribution with cumulative distribution function(CDF)(Figure 7). The CDF plot is following a typical S curve indicative of normal distribution.

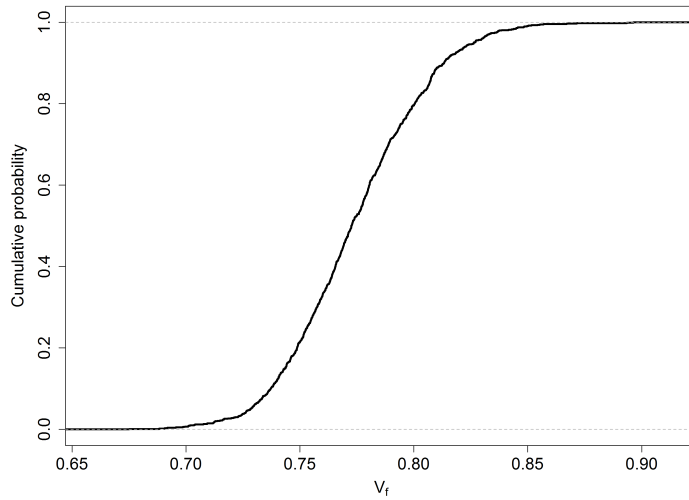


Figure 7: Plot of CDF for local average fibre volume fraction

2.2 The PDF of Permeability (K)

It follows from the section of 2.1 that the fibre volume fraction of a preform, V_f , has a truncated normal PDF, f^{TN} , with mean μ and variance σ^2 over $[V_{f1}, V_{f2}]$ such that $0 < V_{f1} < V_{f2} < 1$:

$$f^{\text{TN}}(V_f) = \frac{\frac{1}{\sqrt{2\pi}} \exp\left(-\frac{(V_f - \mu)^2}{2\sigma^2}\right)}{\Phi\left(\frac{V_{f2} - \mu}{\sigma}\right) - \Phi\left(\frac{V_{f1} - \mu}{\sigma}\right)}, \quad V_{f1} < V_f < V_{f2}. \quad (14)$$

In Eqn. (14) and (15) below, $\Phi(z)$ introduces the distribution function of a standard normal RV Z , that is

$$\Phi(z) = \mathcal{P}(Z \leq z) = \int_{-\infty}^z \frac{1}{\sqrt{2\pi}} \exp\left(-\frac{t^2}{2}\right) dt. \quad (15)$$

Passing to the limits $V_{f1} \rightarrow 0$ and $V_{f2} \rightarrow 1$ Eqn. (14) yields the PDF of normal distribution with mean μ and variance σ^2 .

Now assume the ratio $\frac{r_f^2}{k_c}$ is constant, the RV K is given by an increasing function of V_f , $K = G(V_f)$. Set G^{-1} as inverse function of G , i.e. $V_f = G^{-1}(k)$.

The Figure 2 presents a graphical representation of function G where K is a monotonically increasing function of V_f .

Next, let F_K be the distribution function of RV K , more precisely $F_K(k) = \mathcal{P}(K \leq k)$. Therefore, recalling $K = G(V_f)$ one can do:

$$F_K(k) = \mathcal{P}(G(V_f) \leq k) = \mathcal{P}(V_f \leq G^{-1}(k)) = F_{V_f}(G^{-1}(k)). \quad (16)$$

Where F_{V_f} is the distribution function of V_f . Note that the second probability derives from the of that G is an increasing function of V_f .

Consequently by taking the derivative of F_K with respect to k , the PDF of RV K is obtained by

$$\begin{aligned} f_K(k) &= \frac{d}{dk} F_K(k) = \frac{d}{dk} F_{V_f}(G^{-1}(k)) \\ &= \frac{d}{dk} G^{-1}(k) \cdot f_{V_f}(G^{-1}(k)). \end{aligned} \quad (17)$$

Introduce $k_1 = G(V_{f1})$ and $k_2 = G(V_{f2})$, since G is an increasing function then $0 < k_1 < k_2$. Coming back to the assumption says that the RV V_f has PDF $f^{\text{TN}}(V_f)$ in $[V_{f1}, V_{f2}]$, we obtain

$$\begin{aligned} f_K(k) &= \frac{d}{dk} G^{-1}(k) \cdot f_{V_f}^{\text{TN}}(G^{-1}(k)) \\ &= \frac{d}{dk} G^{-1}(k) \cdot \frac{\frac{1}{\sqrt{2\pi}} \exp\left(-\frac{(G^{-1}(k) - \mu)^2}{2\sigma^2}\right)}{\Phi\left(\frac{G^{-1}(V_{f2}) - \mu}{\sigma}\right) - \Phi\left(\frac{G^{-1}(V_{f1}) - \mu}{\sigma}\right)}, \quad k_1 < k < k_2. \end{aligned} \quad (18)$$

As Figure 2 shows this function is a one to one function so it is invertible. However, while it may be possible to find a closed form solution to this inverse, we will begin by presenting a numerical solution to this problem.

2.3 Numerical results

2.3.1 Statistics of permeability

A summary of statistical properties of permeability for the different COV of V_f is represented in Figure 8. It is observed that an in-plane distribution of local fibre volume fraction results in a distribution of local permeabilities for flow perpendicular to the plane of the fibrous medium. It is established in Figure 8 that domain with larger local average areal densities possess larger local average permeability values. This phenomenon can be explained in terms of probability of number of contact points between fibres. The probability of number of contact points of fibres is larger for the domains with higher local average areal density. Higher contact points means stiffer arrangement of adjacent fibres, causing increased frictional resistance to fluid flow, and hence leading to less permeable area. Furthermore the normalized local average permeability (i) initially decreases when $cv(h)$ increases due to its influence on $cv(V_f)$, (ii) subsequently increases due to the increasing influence of $cv(h)$ on the normalized local average permeability. Therefore, as expected, this implies that the heterogeneity of fibrous media has a significant impact on the magnitude of variation in permeability.

2.3.2 Monte-Carlo simulation

The PDF (18) is computed applying Monte-Carlos simulations (using the "R" statistical software [31]). Monte-Carlo simulation was carried out on the domain with a average fibre volume fraction of 0.78. Subsequently this analytical model fit (18) was compared with what would be predicted by physically based permeability equations (e.g. Kozeny-Carman(2)). To do so, using the values of V_f computed earlier, the distribution of permeability was obtained in (2). Then, probability values calculated through (18) were fit to permeability values. Finally, in order to find the best distribution model to the analytical PDF, different statistical distributions are examined.

Figure 9 shows, obtained through the method described above, (i) the data are not symmetric and skewed to the right, (ii) there is significant agreement between the analytical approach and the simulation results of permeability (Kozeny-Carmen). The observed skewness in permeability distribution is close to what one was observed in [32] at macrolevel. The same principle was applied to various kinds of correlations between K and V_f . Table 2 lists the distribution behaviour of K derived from models found in the literature. The appearance of the distributions presented in table 2 is the same as one shown in Figure 9.

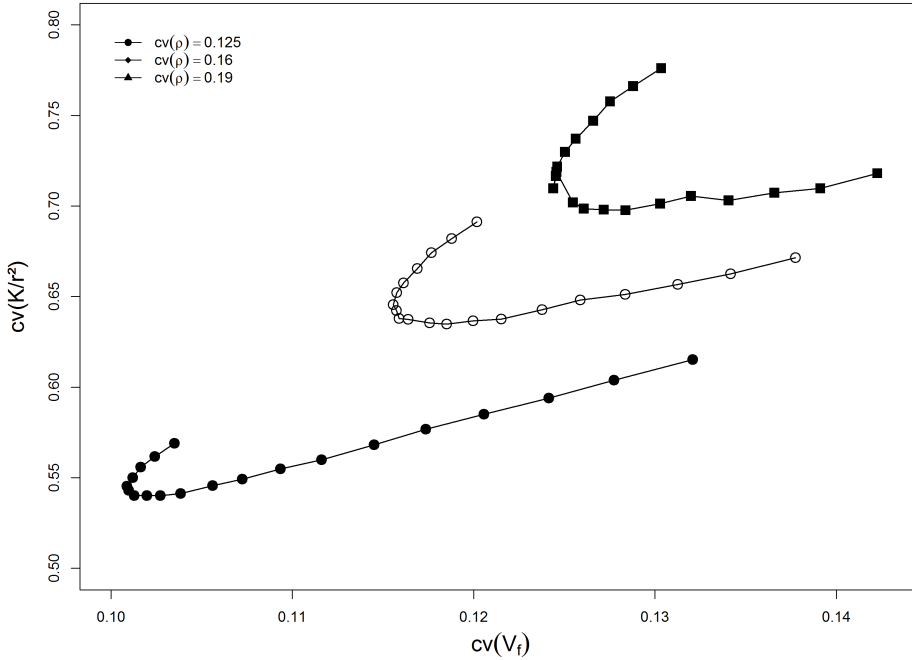
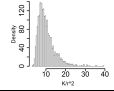
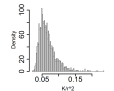
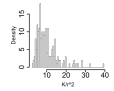
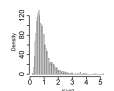
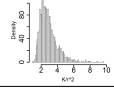
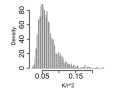
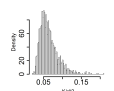


Figure 8: the normalized local average permeability against coefficient of variation of local fibre volume fraction.

Table 2 shows that the skewness of K lies between 1.78-3.45, implying non-normal distribution of the permeability. In addition, the kurtosis values range between 9 and 24, deviating extremely from normality. As expected, there is a significant difference between the calculated skewness and kurtosis and that of the normal distribution.

Furthermore, Figure 10 illustrates how well the different distributions including normal, lognormal, gamma, and beta fit to the analytical probability function. It is clear that the normal and beta distributions fail to represent the distribution of permeability values. Figure 10 also shows a lognormal distribution as well as a gamma distribution provide a good fit for permeability values. It has been derived that both lognormal and gamma distributions can be used effectively in analyzing a non-negative right-skewed data set [39]. As shown in Figure 10, a comparison between the lognormal and gamma distributions reveals that their PDFs have similar results. To find which of these distributions gives better fit to the data, we have considered two data transformation methods, one based on the normal approximation to the log of the data set, working on lognormal distributions and the other based on the cube root of the data, working on gamma distribution: If the data looks symmetric after log transformation, the lognormal distribution would work better to represent the variation of the permeability. If the

Table 2: Comparison of distribution of normalized permeability for different empirical equations

References	K/r^2	Goodness of fit		
		Histogram	Skewness	Kurtosis
Gebart(Square) (1992)[33]	$\frac{16}{9\pi\sqrt{2}}(\sqrt{\frac{\pi}{4V_f}} - 1)^{2.5}$		2.22	12.22
Gebart(Hexagonal) (1992)[33]	$\frac{16}{9\pi\sqrt{6}}(\sqrt{\frac{\pi}{2\sqrt{3}V_f}} - 1)^{2.5}$		2.12	11.53
Bruschke and Advani (1993)[34]	$\frac{1}{3} \frac{(1-L)^2}{L^3} \left(\frac{3L \arctan \sqrt{\frac{1+L}{1-L}}}{\sqrt{1-L^2}} + \frac{1}{L^2} + 1 \right)^{-1}$, (where $L^2 = 4V_f/\pi$)		3.45	24.15
Gutowski et al. (1987)[35]	$\frac{1}{V_f^2} \frac{(0.76 - V_f)^3}{0.76 + V_f}$		3.11	20.38
Happel (1959)[36]	$\frac{1}{9V_f} \frac{6 - 9V_f^{0.33} + 9V_f^{1.67} - 6V_f^2}{3 + 2V_f^{1.67}}$		1.94	10.208
Lee and Yang (1997)[37]	$\frac{1}{8} \frac{(0.7854 - V_f)(1 - V_f)}{V_f^{1.3}}$		2.01	10.63
Sharaoui and Kaviany (1992)[38]	$\frac{0.0602\pi(1 - V_f)^{5.1}}{V_f}$		1.78	9.006

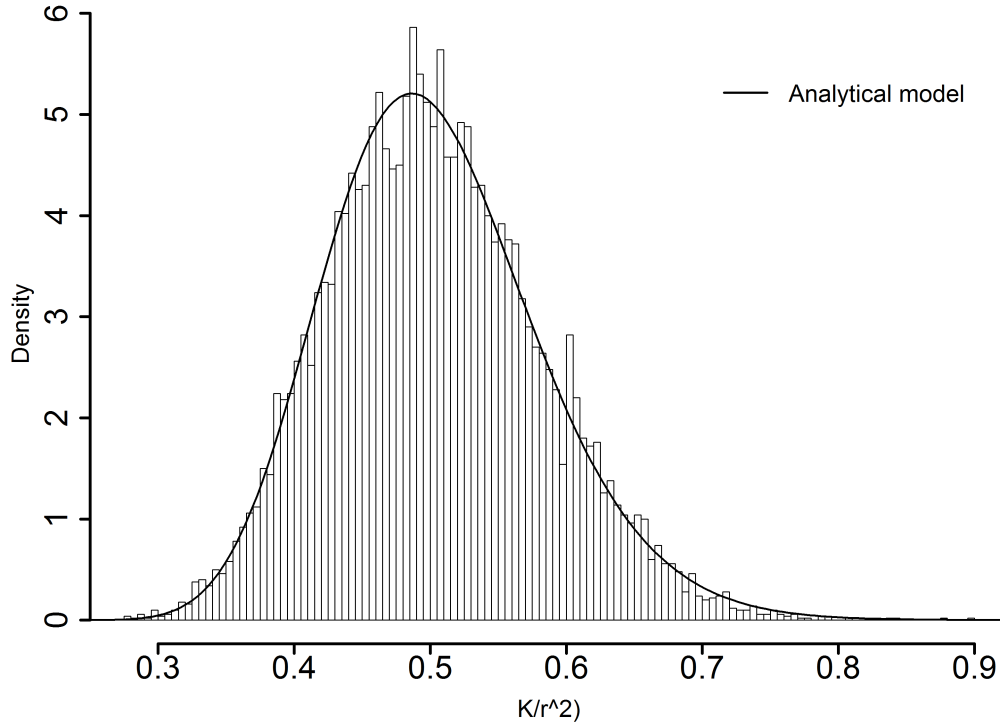


Figure 9: Fitting the computed PDF to histogram of the predicted permeability from Kozeny- Carmen

data looks symmetric after the cube root transformation, the gamma distribution would work better to represent the variation of the permeability [40].

According to Figure 11, although the log transformation seems to fit well in the body of permeability values, the data shows to be left-skewed on log scale. The significant left-skewed on log scale also is observable on the work of Zhang et al.[14](see Figure 12), who evaluated the permeability from local areal weight combined with the Kozeny-Carmen model, suggesting that the lognormal distribution can be used to describe the permeability distribution.

One final comment on which we would like to conclude this section regards entropy. In the literature it has been proven that under constraints, known mean and variance, the normal distribution maximizes entropy. Using this principle that maximizes entropy is a selecting factor for a model we calculated the entropy values of the two fits. Using straightforward computations we obtain the entropies for lognormal PDF -0.931 and gamma PFD -0.887, which coincides with the previous result claiming gamma distribution with more entropy determines the permeability data

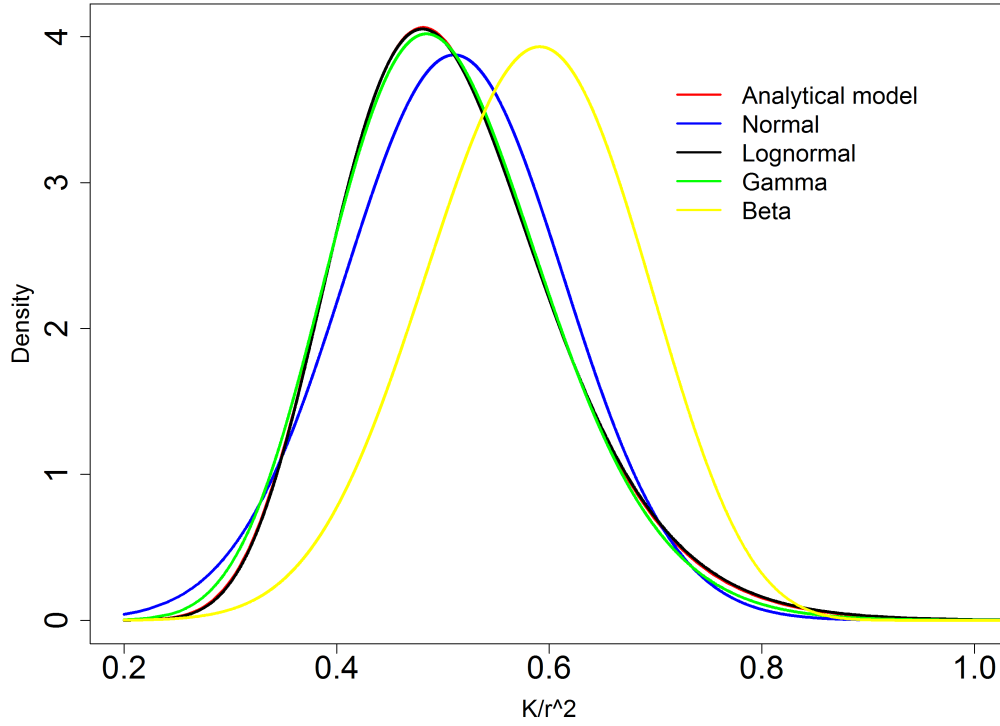


Figure 10: Comparing the computed PDF with common density functions

2.3.3 Applicability of the gamma distribution

In order to examine the applicability of gamma distributions to other empirical permeability equations, these equations are subjected to the Kolmogorov-Smirnov Statistics (KSS) test for normality in terms of normal, lognormal, gamma, weibull and beta distributions. If, in the KSS test $P < 0.05$, there is significant probability of deviation from normality. The P value computations are listed in Table 3. Gamma distribution shows the largest P-values among the given distributions for the different empirical permeability equations. Hence, based on the information in Table 3, we conclude that the gamma distribution provides the best fit. Furthermore, it is shown in Table 3 the permeability COVs of all empirical equations range between 0.43 and 0.74, which is about 8 times larger than the fibre volume fraction COV of 0.086. This suggests that permeability is subjected to larger uncertainty than fibre volume fraction.

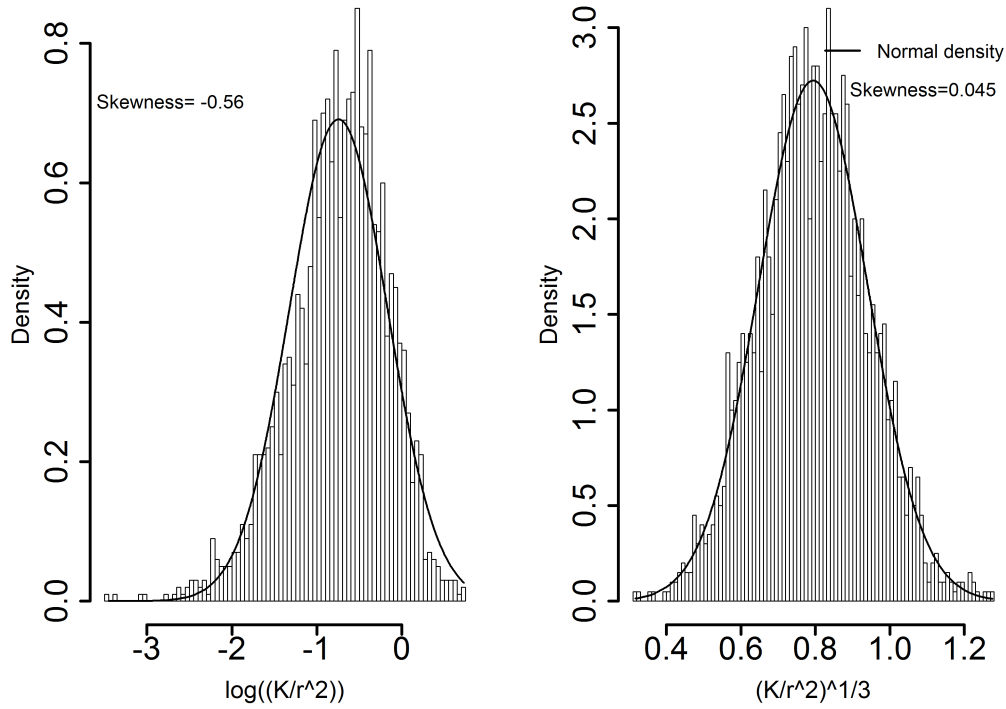


Figure 11: Fitted normal densities for the two scenarios of transformation. The plot on the left side is based on logtransformation and the plot on the right side is based on the cube root transformation

Table 3: Applicability of gamma distribution for different empirical equations

References	Permeability COV	KSS test				
		Normal	Lognormal	Gamma	Weibull	Beta
Kozeny-Carmen (1937)[1]	0.475	4.67e-13	4.435e-5	0.346	2.97e-06	1.017e-09
Gebart(Square) (1992)[33]	0.554	6.106e-15	1.285e-8	0.05244	0.0003844	2.2e-16
Gebart(Hexagonal) (1992)[33]	0.439	4.902e-11	4.96e-6	0.1171	1.526e-05	0.04888
Bruschke and Advani (1993)[34]	0.52	4.6e-14	0.000114	0.2883	1.307e-6	1.58e-8
Gutowski et al. (1987)[35]	0.739	<2.2e-16	2.213e-9	0.2948	0.0007611	0.04888
Happel (1959)[36]	0.44	2.112e-8	1.32e-5	0.1697	.0003369	0.004764
Lee and Yang (1997)[37]	0.53	7.809e-12	1.62e-7	0.1209	0.0031	0.000438
Sharaoui and Kaviani (1992)[38]	0.54	<2.2e-16	< 2.2e-16	0.2336	0.0018	0.000238

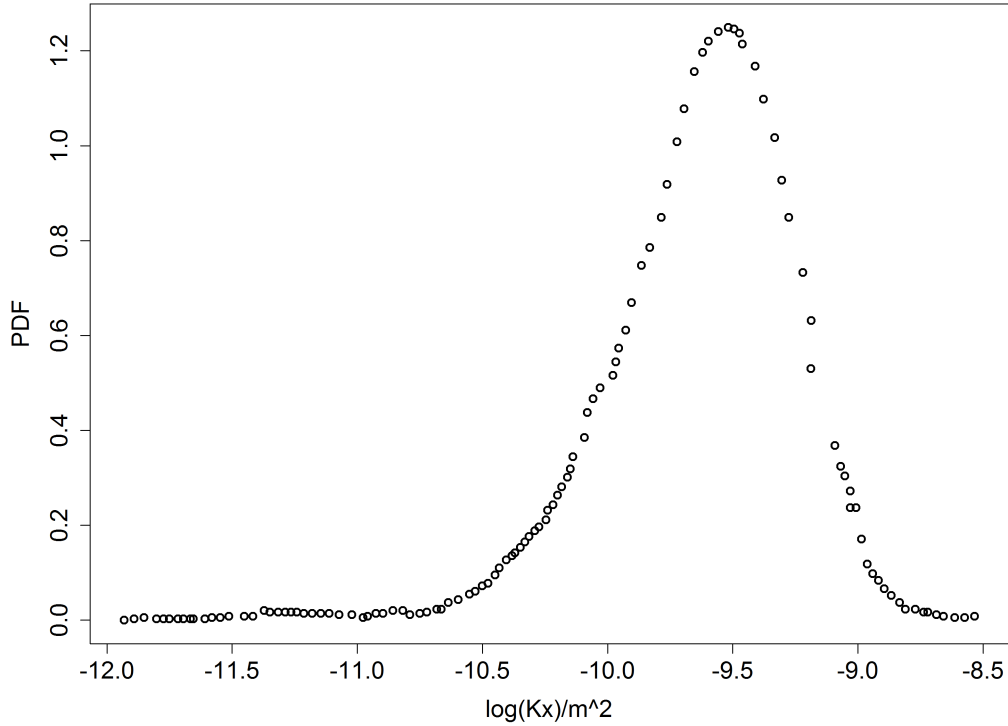


Figure 12: PDF of permeability[14]

3 Conclusions

An adequate representation of microstructural variability of fibre arrangement in fibre-reinforced composites is of critical importance for the analysis of the flow in the fibrous media. The Distribution of fibre volume fraction was quantified by the measurement of areal weight density and areal thickness from optical images of tows in a 2×2 twill carbon-epoxy composite. Then, the PDF of the permeability was determined by a known PDF of V_f and assuming a constant k_c . To do so, we proposed a method to determine the probability density function of the permeability of porous media. We employed the Kozeny-Carmen equation and combined it with the change of variable technique. Our results suggest that (1). The relationship between the local areal weight density and thickness is well approximated by a bivariate normal distribution. (2). The distribution of local fibre volume fraction exhibits a bell-shaped curve and fit well to a normal distribution model. (3). Assuming constant k_c , a gamma distribution could more accurately describe the variation in permeability data.

As conclusion, the understanding of the probability distribution of permeability is still taking further clarification but that the hypothesis of normality has been refuted.

Acknowledgement

SYS thanks the CAPES PNPD-UFSCAR Foundation for the financial support in the year 2014-5. SYS thanks the Federal University of Sao Carlos, Department of Statistics, for hospitality in 2014-5.

References

- [1] Carmen P. Fluid flow through a granular bed. *Transactions of the institution of chemical engineers* 1937; 15:150–167.
- [2] Wong C, Long A. Modelling variation of textile fabric permeability at mesoscopic scale. *Plast Rubber Compos* 2006; 35(3):101–111.
- [3] Mesogitis TS, Skordos AA, Long AC. Uncertainty in the manufacturing fibrous thermosetting composites: A review. *Composite part A: Applied science and manufacturing* 2014; 57:67-75.
- [4] Bodaghi M, Gonçalves CT, Correia NC. A quantitative evaluation of the uncertainty of permeability measurements in constant thickness fibre reinforcement. *In: proceedings of ECCM-16 conference. Seville* June, 2014.
- [5] Arbter R, et al. Experimental determination of the permeability of textiles: A permeability benchmark exercise. *Composite part A: Applied science and manufacturing* 2011; 42:1157-1168.
- [6] Vernet N, et al. Experimental determination of the permeability of engineering textiles: Permeability benchmark II. *Composite part A: Applied science and manufacturing* 2014; 61:172-184.
- [7] Pan R, Liang Z, Zhang C, Wang B. Statistical characterization of fibre permeability for composite manufacturing. *Polymer Composites* 2000; 21(6): 996-1006.
- [8] Hoes K, Dinescu D, Sol H, Vanheule M, Parnas RS, Luo Y, Verpoest I. New set up for measurement of permeability properties of fibrous reinforcements for RTM. *Composite part A: Applied science and manufacturing* 2002; 33:959-969.
- [9] Li J, Zhang C, Liang Z, Wang B. Stochastic simulation based approach for statistical analysis and characterization of composites manufacturing processes. *Journal of manufacturing systems* 2006; 25(2): 108-121.
- [10] Endruweit A, Long AC, Robitaille F, Rudd CD. Influence of stochastic fibre angle variations on the permeability of bi-directional textile fabrics. *Composite part A: Applied science and manufacturing* 2006; 37:122-132.

- [11] Wong CC. Modelling the effects of textile preform architecture on permeability. *PhD thesis, University of Nottingham, Nottingham, England* 2006.
- [12] Padmanabhan SK, Pitchumani R. Stochastic modelling of nonisothermal flow during resin transfer moulding. *International journal of heat and mass transfer* 1999; 42:3057-3070.
- [13] Zahng F, Cosson B, Comas-Cardiba S, Binetruy C. Efficient stochastic simulation approach for RTM process with random fibrous permeability. *Composites science and technology* 2011, 71:1478-1485.
- [14] Zahng F, Comas-Cardiba S, Binetruy C. Statistical modelling of in-plane permeability of non-woven random fibrous reinforcement. *Composites science and technology* 2012;72(12):1368–79.
- [15] Parseval Y, Roy RV, Advani SG. Effect of local variations of preform permeability on the average permeability during resin transfer molding of composites. *ANTEC'95* 1995;2:3040-3044.
- [16] Gebart B.R. Permeability of unidirectional reinforcements for RTM. *Journal of composite materials* 1992, 26:1100-1133.
- [17] Sahraoui M, kaviany M. Slip and no-slip boundary conditions at interface of porous, plain media. *Journal of heat and mass transfer* 1992, 35:927-94.
- [18] Bruschke M., Advani S.G. Flow of generalized Newtonian fluids across a periodic array of cylinders. *Journal of rheology* 1993, 37:479-498.
- [19] Westhuizen J.V.D, Plessis J.P.D. An attempt to quantify fibre bed permeability utilizing the phase average Navier-Stokes equation. *Composite part A: Applied science and manufacturing* 1996, 27A:263-269.
- [20] Lee S.L, Yang J.H. Modeling of Darcy–Forchheimer drag for fluid flow across a bank of circular cylinders. *International journal of heat and mass transfer* 1997 40:3149-3155.
- [21] Catalanotti G, Bodaghi M, Correia N. On the statistics of transverse permeability of randomly distributed fibres. *Submitted to journal of science and technology* 2015; under review.
- [22] Yu B. Analysis of flow in fractal porous media. *Applied mechanics reviews* 2008, 61: 050801-1-19.
- [23] Haldar A, Mahadevan S. Probability, reliability, and statistical methods in engineering design. *ohn Wiley, New York* 2000.
- [24] Stuart A, Ord K. *Kendall's Advanced Theory of Statistics* 1998; Arnold, London, 6th Edition, Vol 1: p. 351.

- [25] Elandt-Johnson R C, Johnson N L. *Survival Models and Data Analysis* 1980; John Wiley and Sons NY, p. 69.
- [26] Hinkley D V. On the ratio of two correlated normal random variables. *Biometrika* 1969; 56 (3): 635-639.
- [27] Cedilnik A, Košmelj K, Blejec A. Ratio of two random variables: A note on the existence of its moments. *Metodološki zvezki* 2006; 3 (1): 1-7.
- [28] Xie Y, Jie Q. A new efficient ellipse detection method. *IEEE* 2002; 1051: 4651-4652.
- [29] Basca C.A, Talos M, Brad R. Randomized hough transform for ellipse detection with result clustering. *IEEE* 2005; 1397-1400.
- [30] Dodson C, Oba Y, Sampson W. On the distributions of mass, thickness and density in paper. *Appita J* 2001,54:385-389.
- [31] Team, R.D.C. R: A language and environment for statistical computing. *Vienna, Austria: R foundation for statistical computing* 2010.
- [32] Liu Q, Parnas R.S, Giffard H.S. New set-up for in-plane permeability measurement *Composite part A: Applied science and manufacturing* 2007, 38:954-962.
- [33] Gebart B.R. Permeability of unidirectional reinforcements for RTM. *Journal of composite materials* 1992, 26:1100-1133.
- [34] Brusckhe B.R, Advani S.G. Flow of generalized Newtonian fluids across a periodic array of cylinders. *Journal of rheology* 1993, 37:479-498.
- [35] Gutowski T.G, Cai Z, Bauer S, Boucher D, Kingery J, Wineman S. Consolidation experiments for laminate composites. *Journal of composite materials* 1987, 21:650-669.
- [36] Happel J. Viscous flow relative to arrays of cylinders. *AIChE* 1959, 5:174-177.
- [37] Lee S.L, Yang J.H. Modeling of Dracy-Forchheimer drag for fluid flow across a bank of circular clinders. *International journal of heat and mass transferr* 1997, 40:3149-3155.
- [38] Sharaoui M, Kaviany M. Slip and no-slip boundary conditions at interface of porous, plain media. *International journal of heat and mass transferr* 1992, 35:927-943.
- [39] Johnson, Norman L.; Kotz, Samuel; Balakrishnan, Narayanaswamy. Continuous Univariate Distributions. *Wiley* 1994,1:173.

- [40] E.B.Wilson, M.M.Hilferty.The distribution of Chi-Square. *Proceedings of the nationa academy of sciences* 1931,17:684-688.
- [41] P.Zhang, P.X.K.Song, A.Qu, T.Greene. Effiecient estimation for patient-specific rates of disease progression using nonnormal linear mixed models. *Biometrics* 2008,64:29-38.